Upper and Lower Bounds to Pull-Out Loading of Inclined Hooked End Steel Fibres Embedded in Concrete

David W. A. Rees * and Sadoon Abdallah

Posted Date: 11 June 2024

doi: 10.20944/preprints202406.0617.v1

Keywords: Hooked-end fibre; SFRC; pull-out bounds; transverse isotropy; fibre orientation

 doi:10.20944/preprints202406.0617.v1

Article

Upper and Lower Bounds to Pull-Out Loading of Inclined Hooked End Steel Fibres Embedded in Concrete

David W. A. Rees [1,*] and Sadoon Abdallah [2]

[1] College of Engineering, Design and Physical Sciences, Brunel University London, Uxbridge, London UB8 3PH, UK
[2] Department of Civil Engineering, College of Engineering, University of Anbar, Ramadi, Iraq
* Correspondence: david.rees@brunel.ac.uk

Abstract: Steel fibre reinforced concrete (SFRC) consists of short hooked steel fibres randomly distributed and oriented within the cementitious matrix. The contribution of fibre in bridging cracks to provide the stress transfer required relies upon the orientation of the fibre in the concrete. Bridging fibre aligned with a crack are less effective than those inclined to it. Therefore, understanding the pull-out behaviour of misaligned fibre is a key factor to quantify and optimize the design of SFRC in the structural applications. In the laboratory a single oriented fibre embedded in a solid cylinder of concrete is subjected to a pull-out test where the axis of a tensile force is aligned with the axis of the cylinder. Based upon the observed behaviour this paper presents a new analytical bounding approach to capture the pull-out response of misaligned hooked-end steel fibre embedded in a concrete matrix. The analysis is based upon a transversely isotropic condition assumed for the plasticity that occurs in the cold drawn fibre. The model accounts for the influence of fibre diameter and the combined strengths of the steel and concrete. The model predictions have also been compared with other experimental results published in the literature. The results showed that the model can predict pull-out loads reasonably for different fibre orientations between bounds of failure derived from the strengths of the two constituents. A critical orientation is observed at maximum strength. Therein, an understanding of the pull-out behaviour of misaligned, hooked-end fibres is necessary to optimize the strength of concrete from this method of reinforcement.

Keywords: Hooked-end fibre; SFRC; pull-out bounds; transverse isotropy; fibre orientation

1. Introduction

It is inevitable that concrete structures are subjected to tensile stress during their service lives whether this arises from shrinkage or from flexural bending and shear [1]. Consequently, there is a need to provide the structure with shear strength, flexural strength, ductility, and crack resistance. Because concrete does not have good properties inherently in each regard it needs to be reinforced with an appropriate material in order to render an otherwise weak cementitious structure with the performance required [2]. Steel has always been used and still is the most promising reinforcement as it combines a high tensile strength with a high Young's modulus. High tensile strength steel reinforcement is available as rebar, mesh and fibres [3]. The latter, i.e. short strand steel fibres, are available in different size, shape and alloy type. Of these, hooked end steel fibres have recently received greatest interest among engineers and researchers [4] because of their resistance to being pulled out under tensile loading.

The main contribution from a fibre reinforcement is to absorb tensile without brittle fracture. Tensile stress induced in the cementitious matrix are transferred to the steel fibre by the durable bond characteristics between both basic materials [5]. A fibre, mechanically pre-deformed with hooked ends, bonds to the matrix sufficiently well to resist the pull-out loading. A spread of randomly oriented and distributed fibres can resist micro-cracking at low loads more effectively [6]. For an individual fibre bridging a micro-crack, debonding starts along its short, 50 mm straight length under

 doi:10.20944/preprints202406.0617.v1

low loads. With increased loading a full debonding occurs [7]. There follows further micro-cracking leading, eventually, to the formation a macro-crack. The bond mechanisms involved between fibre and matrix have been investigated to improve the mechanical performance of steel fibre reinforced concrete (SFRC) [8]. Here the interaction between interfacial bonds across many fibres in a cementitious matrix becomes active in providing increased resistance by prolonging the micro-cracking stage [9]. It follows that an SFRC with a large number of fibres contributes more to improving the tensile resistance than another with a lower volume fraction within a similar grade of matrix material.

Numerous analytical and experimental studies have been carried out to investigate the fibre-matrix interfacial properties [10–15]. The majority of these investigations have been devoted to study the bond characteristics when fibres are aligned with the loading direction [16,17]. Relatively few studies have been carried out on the bond behaviour of misaligned fibre reinforcement, which constitutes a more representative practical structure. It appears that the mechanisms governing pull-out behaviour of misaligned fibres differ from those verified experimentally for aligned fibres [18]. In addition to those mechanisms governing pull-out of aligned fibre, i.e. initial de-bonding followed by frictional pull-out, the misaligned fibre introduces fibre bending, matrix spalling and local friction effects.

Some recent studies [19–22] have investigated the mechanisms governing pull-out behaviour of inclined steel fibres in a cementitious matrix. It would appear from these that existing theory is complicated by the many empirical parameters employed to match specific experimental data. Thus, the predictions to a real pull-out condition are questionable across a wide variation in testing procedures that have been adopted in the absence of a standard test. In order to admit this general practical concern theoretical approaches have abounded on the specifics.

Soetens et al. [19] developed a semi-analytical model to simulate the pull-out behaviour of inclined fibres. The accounted for variations in mechanical and geometrical characteristics of the fibre, as well as the influence of fibre orientation

Lee et al. [20] developed an analytical model to predict the pull-out response of inclined hooked-end fibre embedded in an ultra-high strength cementitious matrix. An apparent shear strength and slip coefficient were introduced to express the variation of peak pull-out load and peak slip.

Laranjeira et al. [21] proposed an analytical model to predict pull-out behaviour of the inclined straight and hooked end fibres. A multilinear diagram based on a set of key-points was used to describe the pull-out-slip response. Their model takes account of debonding, friction effects and matrix spalling due to a variation in pull-out inclination.

Zhan et al. [22] developed an analytical model, similar to [21], in which the effect of the hooked-end is captured by a series of key stages in the force versus displacement response during pull-out. The force, calculated for each stage, augments the theoretical force required for the pull out of a straight fibre embedded with similar inclination.

Building upon the investigations reviewed above, it is recognised that relatively few analyses have been made upon the effects of fibre inclination angle upon pull-out force. Hence, the main intention of this paper is to offer an alternative global explanation of the pull-out behaviour that has been observed for inclined, hooked-end steel fibres. The bounding forces found from the present model are validated against new laboratory test results and other published data.

2. Analytical Pull-Out Model for Inclined Hooked-End Fibre

Figure 1a shows a single hooked-end, inclined steel fibre embedded in a concrete matrix. When the fibre orientation lies with an inclination θ to an externally applied tensile force F the stress state within the fibre is not unidirectional, consisting of axial, transverse and shear components $(\sigma_{11}, \sigma_{22}, \sigma_{12})$ aligned with the fibre co-ordinates (see Figure 1b). Laboratory testing of an inclined fibre provides the pull-out force F applied horizontally to half the length of a single-hooked-end, embedded fibre for a useful inclination range: $0 \leq \theta \leq 90^{\circ}$ in the manner of Figure 2a. It is expected that the pull-out force first breaks the interface bond under a complex stress state in a similar manner to that explained above for a straight fibre. Then, with the fibre freed from the matrix, the fibre shank's

Preprints.org (www.preprints.org) | NOT PEER-REVIEWED | Posted: 11 June 2024 doi:10.20944/preprints202406.0617.v1

stress components shown (enlarged in Figure 1b) are provided by a simpler off-axis stress transformation under the uniaxial loading [23].

$$\sigma_{11} = \sigma \cos^2 \theta \quad (1a)$$

$$\sigma_{22} = \sigma \sin^2 \theta \quad (1b)$$

$$\sigma_{12} = (\sigma/2) \sin 2\theta \quad (1c)$$

where $\sigma = F/A$ is the applied stress, found from the fibre section area A over which F is distributed uniformly at its half-length entry position in Figure 2a.

Fig.1a

Fig.1b

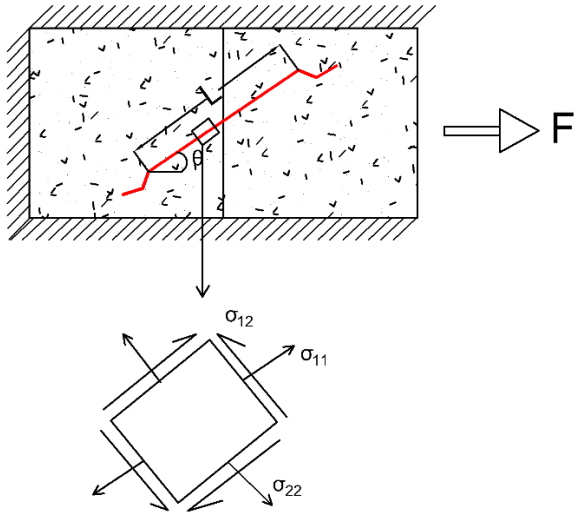

Figure 1. Stress state for inclined hooked-fibre embedded in cementitious matrix.

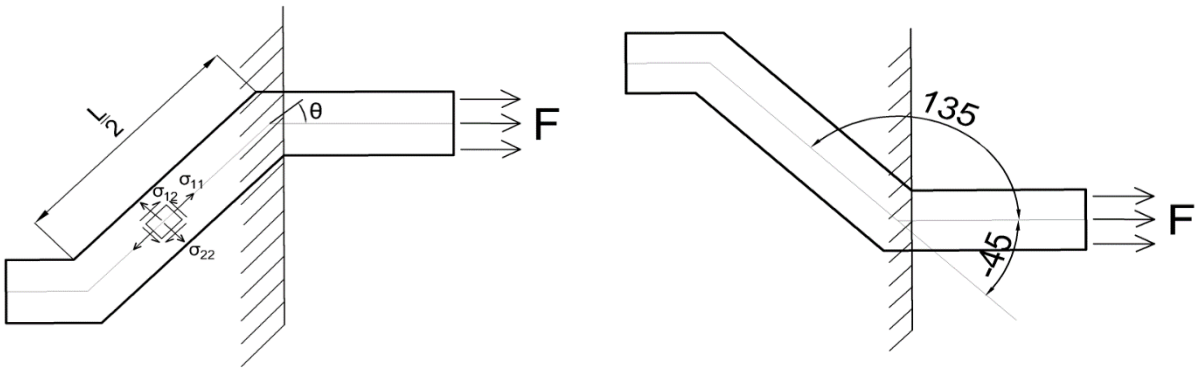

(**a**) (**b**)

Figure 2. Alternative left side half length arangement used for (**a**) experiment and (**b**) bond failure prediction**.**

2.1. Fibre Failure Criteria

The transversely isotropic condition assumed here for the cold drawn wire itself, is similar to that which applies across a transverse section of a composite material in which many unidirectional fibres are embedded in a polymer resin matrix [24]. This composite has isotropic properties for all orientations in the plane of the section, 2-3 in Figure 3a, but is anisotropic, i.e. direction dependent, for its two remaining orthogonal planes 1-2 and 1-3.

Preprints.org (www.preprints.org) | NOT PEER-REVIEWED | Posted: 11 June 2024 doi:10.20944/preprints202406.0617.v1

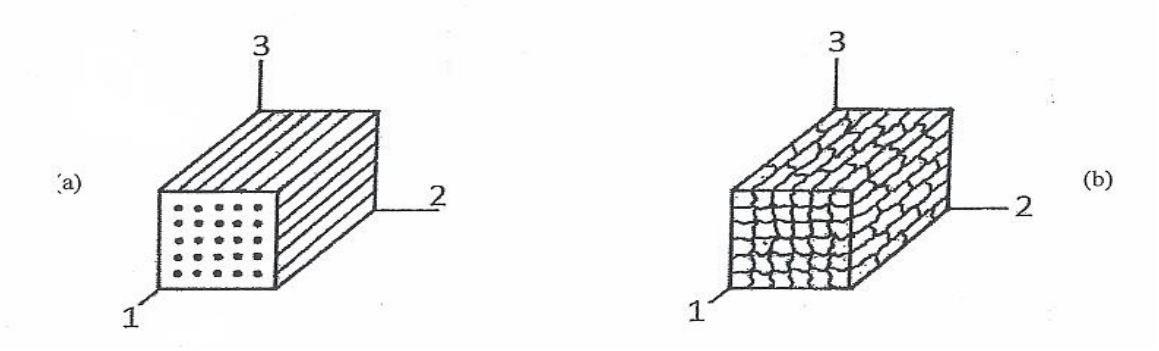

Figure 3. Transversely isotropic plane (2B3) for (**a**) unidirectional fibres (**b**) extruded grains.

Rolled sheet and cold drawn metal wire has similar character to Figure 3a but to a lesser degree. Thus, in the plane 2B3 of the fibre cross-section, in Figure 3b the polycrystalline grains appear equiaxed and isotropic. However, in the extruded or cold drawn direction (planes 1B2 and 1B3) elongated grains exhibit direction-dependent properties similar to a unidirectional reinforced composite. Hence, a transversely isotropic failure criterion is assumed for the fibre, deep drawn to its final diameter (0.9 mm), having had its grains elongated by multiple reductions. Metallography revealed (see Figure 4a) elongated grains, aligned with the fibre=s drawn direction 1, with an aspect ratio exceeding five. Figure 4b shows less directionality within a cross section of an isotropic plane of the cross-section. The equiaxed grains that appear have an average diameter of 2 μm approximately. Clearly, there are variations in grain size but these do not appear in the macroscopic plasticity theory required for: (i) a shank failure criterion at ultimate strength and (ii) straightening the fibre's hooked ends during pull-out. from the matrix.

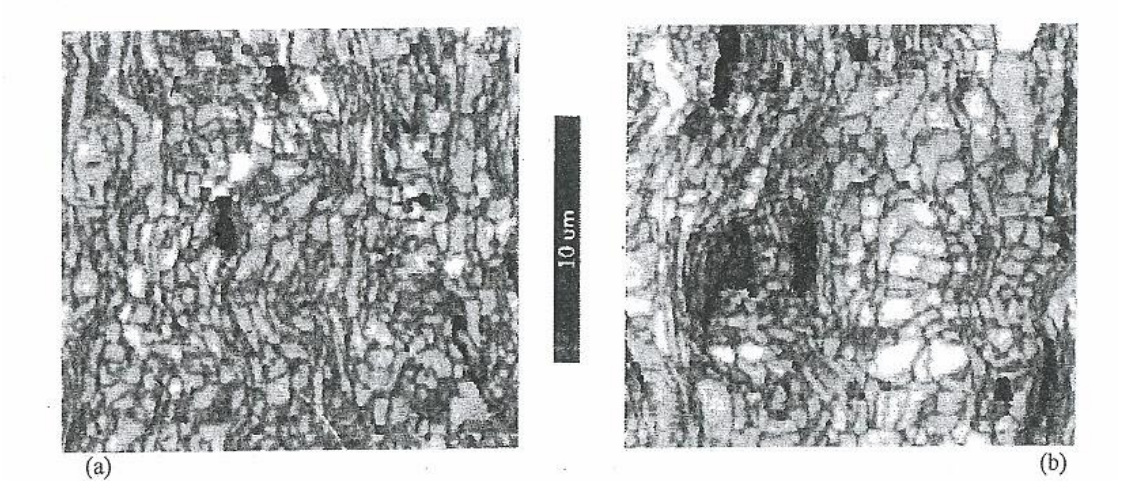

Figure 4. Grain structures: (**a**) elongated (**b**) transverse isotropy for deep drawn fibre.

2.1.1. *Transverse Isotropy*

Where in Figure 2a the straight shank axis of a pre-bent fibre lies with an inclination θ to an applied tensile stress: $\sigma = F/A$, a plane stress state (Equations (1a–c)) exists within the fibre. Correspondingly, the fibre's >off-axis= failure criterion for the plane stress state, shown in Figs. 1b and 2a, appears in a non-dimensional form [25]:

$$\sigma_{11}\,(\,\sigma_{11}\,!\,\sigma_{22})\,/\,\sigma_{1f}{}^{2} + \sigma_{22}{}^{2}/\sigma_{2f}{}^{2} + \sigma_{12}{}^{2}\,/\,\sigma_{12f}{}^{2} = 1 \qquad (2a)$$

where σ_{1f}, σ_{2f} and σ_{12f} are, respectively, the ultimate strengths of the fibre in axial tension, transverse tension and shear. Substituting Equations (1a-c) into Equation (2a) provides an off-axis failure criterion in terms of the applied tensile stress and the fibre inclination:

$$(\sigma^{2}\cos^{2}\theta\,/\sigma_{1f}{}^{2}\,)(\cos^{2}\,\theta\,!\,\sin^{2}\,\theta) + (\sigma^{2}\sin^{4}\theta)\,/\,(\sigma_{2f}{}^{2}) + (\sigma^{2}\sin^{2}2\theta)\,/\,(4\sigma_{12\,f}{}^{2}\,) = 1 \qquad (2b)$$

 doi:10.20944/preprints202406.0617.v1

in which $\sigma = \sigma_\theta = F/A$ is the applied tensile stress in the fibre with an inclination θ. Re-arranging Equation (2b) provides the limiting applied stress (failure stress) σ_θ for an inclined fibre B written in a normalised form to enable the off-axis strength to be compared more conveniently with experimental data:

$$(\sigma_\theta / \sigma_{1f})^2 [\cos^2\theta \cos 2\theta + (\sigma_{1f} / \sigma_{2f})^2 \sin^4\theta + (1/4) (\sigma_{1f} / \sigma_{12f})^2 \sin^2 2\theta] = 1 \qquad (3)$$

As a check upon Equation (3), the oriented strengths in tension, compression and shear are provided by orientations $\theta = 0°$, 90° and 45° respectively:

$$\theta = 0°; (\sigma_{0°}/\sigma_{1f})^2 = 1, \square\ \sigma_{0°} = \sigma_{1f}$$

$$\theta = 90°; (\sigma_{90°}/\sigma_{2f})^2 = 1, \square\ \sigma_{90°} = \sigma_{2f}, \sigma_{90°}/\sigma_{1f} = \sigma_{2f}/\sigma_{1f}$$

$$\theta = 45°; (1/4) (\sigma_{45°}/\sigma_{12f})^2 = 1, \square\ \sigma_{45°} = 2\,\sigma_{12f}, \sigma_{45°}/\sigma_{1f} = (2\sigma_{12f}/\sigma_{1f})$$

An isotropic prediction (von Mises) from Equation (3) applies when: $\sigma_{1f}/\sigma_{2f} = 1$ and $\sigma_{1f}/\sigma_{12f} = 3$:

$$\sigma_\theta/\sigma_{1f} = (\cos^2\theta \cos 2\theta + \sin^4\theta + (3/4) \sin^2 2\theta)^{1/2} \qquad (4a)$$

Then, Equation (4a) is equivalent to:

$$\sigma_\theta/\sigma_{1f} = (\sin^2\theta + \cos^2\theta)^{1} = 1 \qquad (4b)$$

which predicts, as expected, a fibre strength that is not orientation dependent. More realistically, anisotropic (orientation dependent) strength ratios between the ultimate strengths in axial tension σ_{1f}, transverse tension σ_{2f} and shear σ_{12f} might be expected to lie in the range:

$$4/3 \# (\sigma_{1f}/\sigma_{2f}, \sigma_{1f}/\sigma_{12f}) \# 2 \quad \text{or} \quad 2 \# (\sigma_{2f}/\sigma_{1f}, \sigma_{12f}/\sigma_{1f}) \# 3 \qquad (5a,b)$$

For example, Figure 5 shows one anisotropic, off-axis plot according to Equation (3) for cold drawn, high strength steel fibre for which the two strength ratios in Equation (5b) are assumed equal to 2. This means that when $\theta = 90°$, $\sigma_\theta = \sigma_{2f} = \sigma_{1f}/2$ at the strength ratio assumed. Equation (3) applies only beyond a critical fibre orientation where the hooked end of the fibre is able to prevent slip by pull-out. Here the fibre shank would fail from having attained its tensile strength in bridging the gap between the free surfaces created by cracking in the concrete matrix. This is unlikely to occur for small orientations given those experiments (3B5) upon aligned fibre which show that when pulled axially a fibre slips out from its matrix accommodated by plastic unhinging of its hooked ends. Here the maximum stress reached in the fibre under the maximum pull-out force is less (the lower bound) than its ultimate strength.

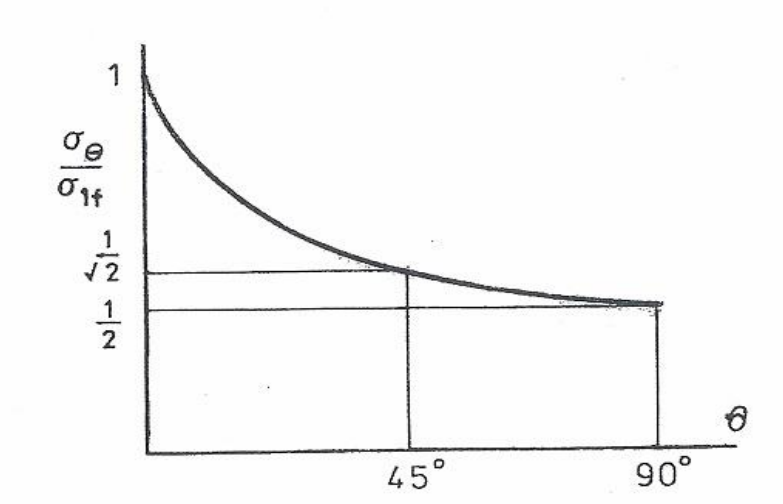

Figure 5. Off-axis strength variation of anisotropic fibre for which $\sigma_{2f}/\sigma_{1f} = \sigma_{12f}/\sigma_{1f} = 2$.

 doi:10.20944/preprints202406.0617.v1

The full strength of an inclined fibre shank is reached (upper bound) only in the absence of matrix spalling (brittle crumbling) upon the crack surface at the fibre=s entry position. Spalling enables the fibre to bend more easily into alignment with the increasing force so widening the gap between the crack surfaces with a reduced embedded length [21]. It is expected, therefore, that an upper bound applies in the absence of spalling in a higher quality cementitious matrix. It follows that inclined fibre pull-out is a complex combination of mechanisms and material behaviour all of which depend upon the inclination in some manner. Despite these difficulties it is possible to simplify critical applied force predictions using a global approach that subsumes these contributory factors. Here the following bounds are placed upon the applied force associated with pull out of inclined fibre and where this is likely to be interrupted with a fibre breakage.

2.1.2. Upper and Lower Bounds

An *upper bound*, giving the maximum pulling force, is provided when, as here, it is based upon the influence of orientation upon the fibre=s nominal strength σ_θ. = F/A. *Note*: Each >transversely isotropic= strength σ_{1f}, σ_{2f} and σ_{12f} in Equation (3) is a fixed material property referred to the 0°, 90° and 45° orientations. The *lower bound* inclined pulling force assumes a slip failure from unhinging at the fibre bend under its axial force component: $F\cos\theta$ in Figure 2a. Thus, an inclined pull-out force is magnified by the factor $1/\cos\theta$ compared to the force required to pull-out a fibre without inclination (i.e. for $\theta = 0°$ in Figure 1a). That is:

$$F_\theta = (F_{0°}/\cos\theta)$$

Here forces F_θ and $F_{0°}$ may be referred to the fibre's cross-sectional area A in a nominal stress:

$$\sigma_\theta = (\sigma_{0°}/\cos\theta) \qquad (6a)$$

A *lower bound* non-dimensional prediction to σ_θ follows from Equation (6a) in dividing by the fibre's axial tensile strength:

$$\sigma_\theta/\sigma_{1f} = (1/\cos\theta)\,(\sigma_{0°}/\sigma_{1f}) \# 1 \qquad (6b)$$

While a *lower bound* $\sigma_\theta/\sigma_{1f}$ can be calculated from Equation (6b) over a full inclination range $0° < \theta < 90°$ it will be cut off at the intersection with an *upper bound* from the failure criterion for an inclined fibre. It has been seen that the failure stress is only constant at all orientations for an isotropic fibre, as Equation (4b) has shown. Otherwise Equation (3) shows that the failure stress σ_θ is orientation dependent, involving a transversely isotropic fibre's anisotropic strength ratios σ_{1f}/σ_{2f} .and σ_{1f}/σ_{12f}. For example, with each ratio at ½, Figure 5 shows that the upper bound failure stress falls with increasing orientation from a maximum of unity corresponding to the ultimate tensile strength (UTS) of aligned fibre ($\theta = 0°$) but this is far greater than the lower bound stress calculated from the force observed for complete pull out of aligned fibre. The inclined force (i.e. nominal stress) resolution has also shown normal and tangential shear stress in Equations (1a–c) acting upon an inclined fibre (see Figure 1b), thereby reducing its resistance to pull-out from a high strength matrix. Where a weaker matrix is damaged around the fibre at entry to a crack surface the re-entrant bending that occurs aids pull out through a pincer action. It is concluded from these observations that a lower bound pull-out force for inclined fibre need not consider opposing influences that promote a slightly greater or lesser value than that found here from basic force resolution. Thus, for design requirements, it is expected that all experimental data would lie between the upper and lower bounds, so obviating the complexity involved in consideration of a more precise marriage of all orientation dependent mechanisms [21]. Taking only the peak loading applies to shallow orientations where a fibre does pull-out fully under a slightly increased force compared to an aligned fibre. However, with increasing fibre orientation the spalling damage it produces in the concrete around the fibre entry aids its release. It is expected here that a fibre rupture occurs consistently at and beyond a critical orientation.

 doi:10.20944/preprints202406.0617.v1

2.1.3. Experimental Data

In Figures 6a-d the peak value of an inclined, applied nominal stress σ_θ is normalised with the UTS (σ_{1f}) for an aligned fibre. It follows from Equation (3) that the uniaxial strength σ_{1f} can never be attained for an embedded inclined fibre failure. Therefore, a restriction must be placed upon the range of strength ratios employed for an upper bound plot. With increasing θ the reduced strength range for inclined fibre failure will appear in the upper bound plot. Upper bounds, shown in Figures 6a-d, are based upon fibres having equal transverse and shear strengths from 50% to 75% of the axial strength, i.e. strength ratios of ½ and ¾ taken from Equation (5b).

It is seen that the upper and lower bounds, predicted from Equations (3) and (5b) capture published data [26B28] on fibre fracture for orientations $30° < \theta \# 60°$ despite the wide variation in fibre diameter and tensile strength (i.e. for Figures 6b, c, and d respectively: 0.5 mm, 1150 MPa [26]; 0.8 mm, 2117 MPa [27]; 1.0 mm, 860 MPa [28]). It appears for these fibres and for the present test data in Figure 6a, for a 0.9 mm fibre with UTS = 860 MPa, that all fibres= strength ratio combinations do lie within the range given in Equation (5a) for their match. These show that a close u. b. fit applies to equal strength ratios: $\sigma_{1f}/\sigma_{2f} = \sigma_{1f}/\sigma_{12f} = 7/4$), assumed in Figure 5. Experimental methods for the determination of strength ratios follow. All results in Figures 6a-d apply to a high strength concrete matrix in which, with spalling effects minimised, embedded fibre shank failures appeared with increasing orientation. Fibre shank failures provide *upper bound* solutions. Otherwise, it is seen that a *lower bound*, pull out prediction from Equation (6b) is adequate for fibre pull-out with lesser orientations in the range $0° \# \theta \# 30°$. With increasing θ a critical σ_θ value divides the bounds, this being found from equating Equations (3) and (6b), for example with $\sigma_{1f}/\sigma_{2f} = \sigma_{1f}/\sigma_{12f} = 2$:

$$(1/\cos^2\theta)(\sigma_{0°}/\sigma_{1f})^2\,(\cos^2\theta\cos2\theta + 4\sin^4\theta + \sin^2 2\theta) = 1$$
$$(\cos2\theta + 4\sin^4\theta/\cos^2\theta + 4\sin^2\theta) = (\sigma_{1f}/\sigma_{0°})^2 \qquad (7)$$

giving, in Figure 6a: $\theta_c \sim 25°$ and $\sigma_\theta/\sigma_{1f} \sim 0.9$, where an aligned fibre intercept value $\sigma_{0°}/\sigma_{1f} = 0.82$ applies to $\sigma_{1f}/\sigma_{2f} = 2$, as shown. In a similar manner other data (see Figures 6bBd), taken from the literature [26–28], lie between the two bounds when normalised with σ_{1f}. *Note*: The nominal, critical applied stress ratio within Figs 6a-d interchanges directly with the ratio between the maximum pull-out/fracture force F_θ and the ultimate tensile force $F_{0°}$ for a 0° fibre of diameter d. That is:

$$F_\theta/F_{0°} = [(\pi d^2/4)\,\mathrm{H}\,\sigma_\theta] / [(\pi d^2/4)\,\mathrm{H}\,\sigma_{1f}] = \sigma_\theta/\sigma_{1f} \qquad (8)$$

Note: $F_{0°} = \sigma_{1f}\,\mathrm{H}\,\pi d^2/4$ is the ultimate tensile force for an aligned fibre. This is found from a standard tensile test in which σ_{1f} identifies with the fibre's UTS. In Equation (8), $F_\theta = \sigma_\theta\,\mathrm{H}\,\pi d^2/4$ refers to either the maximum pull-out load or the fibre shank failure load, as observed from a withdrawal test upon an embedded, inclined fibre. Other tests, that follow, are required to determine the ultimate strength of the fibre in its transverse direction (σ_{1f}) and under shear (σ_{12f}) when the strength ratios, as they appear in Equation (3), are to be determined experimentally.

Preprints.org (www.preprints.org) | NOT PEER-REVIEWED | Posted: 11 June 2024 doi:10.20944/preprints202406.0617.v1

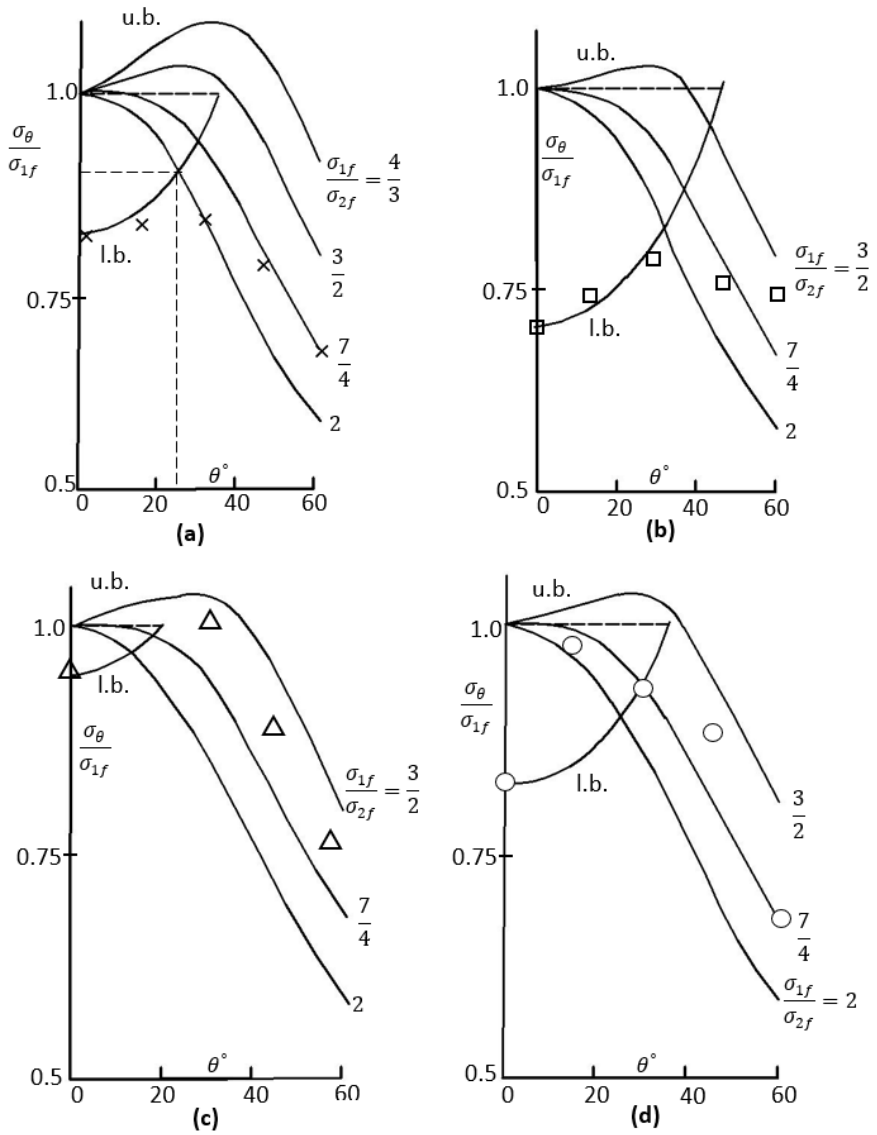

Figure 6. Peak stress dependency upon fibre inclination. Key: (u. b. upper bounds, l. b. lower bound).

2.2. Fibre Strength Tests

High tensile drawn wire is usually supplied with its strength and ductility properties aligned with the length direction. Equation (3) shows that in addition to the axial strength σ_{1f}, the transverse strength σ_{2f} and shear strength σ_{12f} are necessary for an off-axis failure prediction. Wire is usually supplied with its uniaxial tensile strength only, here σ_{1f}. It is most convenient to establish σ_{2f} and σ_{12f} from transverse compression and double shear using indenters between guides in the manner of Figure 7a,b respectively. With an absence of hardening for a high strength 0.9 mm alloy steel wire (supplier Bekaert Dramix), the minimum ultimate transverse strength σ_{2f} is estimated from the load W_E at full elastic compression:

$$\sigma_{2f} = W_E/(bd) \tag{9}$$

where b is the die breadth and d is the wire diameter (see Figure 7a).

 doi:10.20944/preprints202406.0617.v1

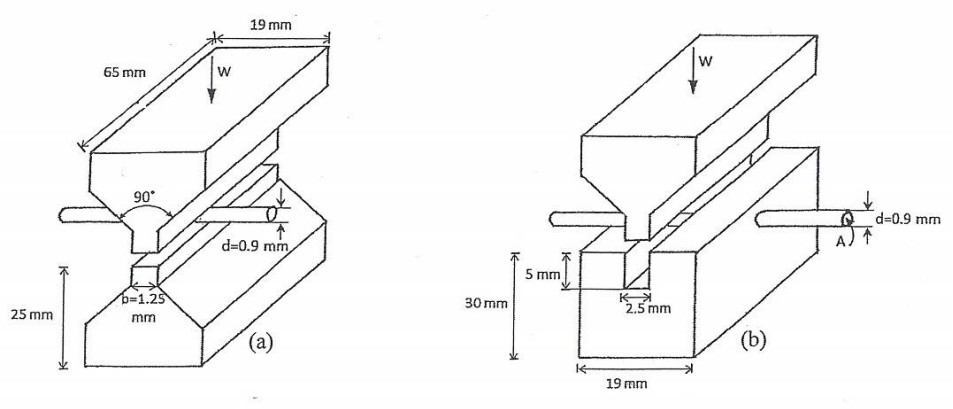

Figure 7. Transverse compression and double shear tests for σ_{2f} and σ_{12f}.

Here, bd is the projected rectangular area under compression lying beneath the die within the wire=s central horizontal plane. A maximum transverse strength applies to the wire=s centre where the principal lateral stresses σ_2 and σ_3 (co-ordinates 2 and 3 in Figure 3b) attain their maxima in compression and tension respectively [29]:

$$\sigma_2 = ! (6W_E\}/(\pi db) \text{ and } \sigma_3 = (2W_E\}/(\pi db)$$

These combine to give a transverse, effective yield strength:

$$\sigma_{2f} = \%(\sigma_2^2 ! \sigma_2\sigma_3 + \sigma_3^2) = (2\%13W_E)/(\pi bd) = (2.3W_E)/(bd) \quad (10)$$

The coefficient 2.3 in Equation (10) is lowered to 2.23 when an axial stress $\sigma_1 = v(\sigma_2 + \sigma_3)$ is taken for the contact zone, with v = 3, to correspond with negligible axial strain from having been constrained by each unstrained length beyond the contact length b.

Ideally, an axial torsion test would be required to determine the shear strength σ_{12f} as requited in Equation (3). The torque required to produce a fully plastic circular section has been well documented [30]. It is given as 4/3 times the yield torque:

$$T_{ult} = 4/3 \text{ H } \pi kr^3/2$$

from which k, the shear yield stress, may be equated to σ_{12f} in the absence of hardening. If a fine wire torsion machine is not available to determine T_{ult} then a transverse shear stress in the plane 2-3 of Figure 3b can be taken as the complement of σ_{12} in Figure 1b. Hence, under double shear (see Figure 7b) the shear strength of fibre is approximated as:

$$\sigma_{12f} = W_S/(2A) \quad (11a)$$

in which there are two wire cross-section areas resisting the total transverse shear load W. More precisely, the maximum shear stress at the centre of a solid circular section under single shear is given by $4W/3A$ [29]. It follows that under double shear the coefficient of 2 in Equation (11a) becomes: 1/2 × 4/3 = 2/3. This gives:

$$\sigma_{12f} = 2W_S/(3A) \quad (11b)$$

Results and calculations of the strength ratios are shown in Table 1. Transverse and shear strength estimates were calculated as described above from Equations (10) and (11b) using a die breadth b = 2.5 mm and high tensile wire of diameter (d = 0.9 mm) supplied with a given axial strength σ_{1f} in three hook geometries.

Table 1. Fibre strengths (MPa) from transverse compression (σ_{2f}) and double shear (σ_{12f}).

Hook(θ°)	σ_{1f}	W_E, **N**	$\sigma_{2f} = 0.99W_E$	σ_{1f}/σ_{2f}	W_S/**N**	$\sigma_{12f} = 1.05W_S$	σ_{1f}/σ_{12f}
3D(60°)	1160	1000	990	1.17	650	682.5	1.70

 doi:10.20944/preprints202406.0617.v1

4D(45°)	1500	1300	1240	1.21	850	892.5	1.68
5D(45°)	2300	2150	2129	1.08	1300	1365	1.80

3. Pull-Out Tests of Inclined Fibres

Figure 8 shows the effect of inclination angle on the maximum pull-out load (F_θ) of inclined hooked end fibres with the following inclinations: 0°, 15°, 30°, 45° and 60°. Those mechanisms governing the pull-out behaviour of inclined hooked end fibre are taken to be similar to those found for aligned straight fibres. These are: initial de-bonding, followed by unbending then frictional pull-out of the straightened fibre. First the force applied must overcome a chemical bonding and frictional resistance from the interface to the fibre. Slip occurs when an increased force releases the mechanical anchorage provided by the hooked end. The unbending required for this release occurs involves plastic deformation within hinges that form successively at each bend of the fibre hook. When straightened the completed pull out of the fibre occurs under a much lower force that equates to any remaining sliding friction. The mechanical anchorage contribution provided by a hooked end fibre increases the pull-out load after de-bonding significantly. In contrast, following debonding of an embedded straight fibre only frictional resistance remains to be overcome under a falling load. The pull-out load versus slip responses shown in Figure 8 reveal the load variations found from separate pull out tests upon hooked-end fibres at five orientations.

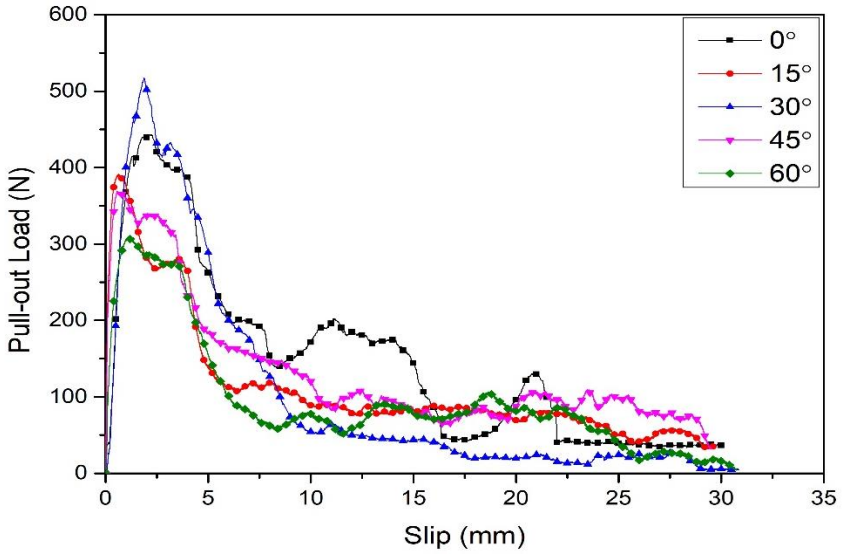

Figure 8. Pull-out load vs slip of inclined hooked end fibre.

The pull-out plots are often presented as an average of a number of tests conducted under similar controlled test conditions of temperature, straining rate, loading alignment and consistency of material composition. Though the averaging has removed vibrational scatter in the loading an irregularity remains in each plot which can defy an accurate prediction. Despite this, most reports on pull-out testing continue to identify a sequence of failure events within the plot of pull-out load versus fibre slip [1–20]. The first event is the region along a rising curve within which fibre de-bonding has occurred. Thereafter, each flat load plateau is identified [20] with the bending required to straighten the fibre hook prior to its complete removal from the matrix at a slip displacement, which equals 30 mm as a straightened embedded length (see Figure 8). The anchorage offered by the hooked end raises the load to the maximum observed as required for straightening the fibre at its first bend. Thereafter, lower load plateaus have been associated, successively, with bending at the trailing ends of the hook as necessary for the fibre to slip further in the straight region of the matrix tunnel. Some erosion of that straight region occurs with spalling in the matrix around the fibre at its exit surface. Therein, with some loss of fibre orientation, further load plateaus appear less distinct,

 doi:10.20944/preprints202406.0617.v1

where the number of these depends the hook design. Spalling becomes more severe in fibre with larger inclination to the pulling force. A bending of fibre in a spalled surface cavity leads to premature failure [18–21] of the fibre before its complete removal. Such behaviour has motivated the present bounding approach to admit steeper fibre inclinations under loading where fibre fracture interrupts its complete withdrawal. Invoked by the bounding approach the critical load for an incomplete pull-out, i. e. from fibre fracture, lends itself to a division between its upper and lower bound limits. It is also suggested here that a further intermediate bound be placed upon the tensile strength of the concrete at the interface region where spalling occurs. The ratio of tensile strength of concrete is a small fraction of that for the steel fibre. Consequently, spalling would be expected to occur around the fibre's entry position to a freed crack surface under a relatively low pull-out load. This behavior arises in practice where a randomly orientated fibre distribution serves to bridge free crack surfaces that arise in a concrete matrix under service loading conditions, i.e. the primary role of reinforcement. In serving that role a bridging fibre(s) with orientation would be more likely to create a spalling cavity than an aligned fibre. Pulling on a mis-aligned fibre creates a bending moment at entry to the matrix. Quite apart from its contribution to fibre failure, this bending imparts both tension and compression to the surrounding matrix, with the concrete on its tensile side being most likely to spall. There may appear opposing force at work here! While spalling acts to lessen resistance to pull out the shank inclination increases that resistance in a lower bound mode (see Figure 6a-d). Conversely, the upper bound mode shows that a shank failure stress is reduced as the plane stress state (Figure 2a) within it is accentuated by the fibre's orientation. The interplay between such influences upon the failure stress (i.e. the 'pull-out force per unit area) depends upon orientation in a manner suggested from bounding failures: a lower bound failure from complete pull-out of slightly mis-alignment fibre; an upper bound shank failure for misaligned fibre beyond a critical orientation. In Figs 6a-d the unit ordinate cuts off a l. b. failure i.e. when the applied stress attains the ultimate strength of the fibre. Experiment shows that this condition is never attained. Thus, with the straightening of the hook end, preceding its complete withdrawal, the applied stress is found to be less than the ultimate strength. Fibre pull-out would appear to be most consistent with an aligned stress condition. The implication drawn from Figure 6 is that a l. b. fibre pull-out applies only to low range of 'misaligned' fibre. Figure 6 suggests safely that a range of $\theta < 10^{\circ}$ applies to a l. b. pull-out plot before it is intercepted by an upper-bound fibre failure. The latter requires less loading to be applied for failure in fibre with increasing orientation as the stress components seen within the plane stress state of Figure 1b increase. Thus, a combined stress failure in an off-axis fibre occurs under an applied load less that the load required for a uniaxial tensile failure of an aligned fibre. The combined loading may also involve flexure of a fibre within a spalled cavity and further surface shear from any fibre slip from within the surrounding matrix. Again, each influence would contribute to combined stress yielding under a lower applied load compared to the load necessary for uniaxial yielding to occur. Experimental data lends support to the yield criterion. It can be seen from Figure 9 that the maximum pull-out load at 15° and 30° fibre shank inclinations are 3.2% and 5.3% higher than that for an aligned fire shank (0°). At 45° and 60° inclinations, the maximum pull-out load is 20.2 % and 36.8 % less than that of the aligned fibre. The maximum pull-out load of hooked end fibre increased with inclination angle up to 30° in accordance with the lower bound Equation (6b). At greater inclinations 45°and 60° an upper bound failure occurs assisted by spalling. Here with a fibre failure the full deformation is reached in the shank at ultimate strength, before the end can straighten to facilitate pull-out. Despite the change in failure mode it is seen that the upper bound loading remains high within the orientation dependent strength of cold drawn steel fibre. Lower bound loads do involve plastic hinging under flexure but at lower loading than that required to produce an off-axis tensile shank failure.

 doi:10.20944/preprints202406.0617.v1

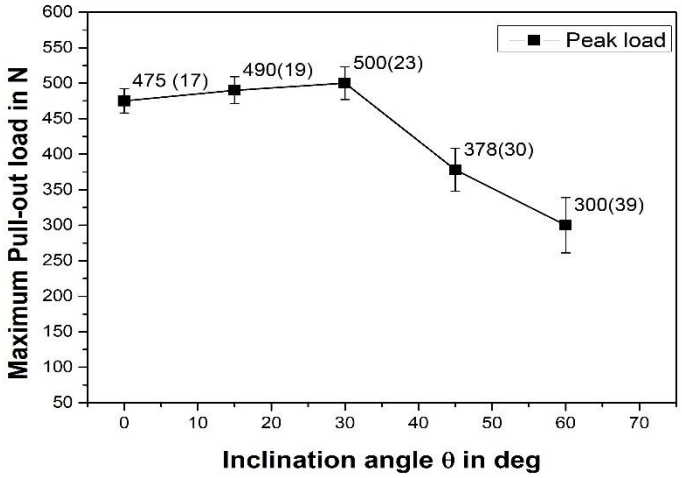

Figure 9. Maximum pull-out load vs inclination angle.

The maximum pull-out load appears for a fibre inclination of 30°. This has been explained in a change in deformation mode from plastic unhinging in the hook to shank plasticity, the latter reminiscent of triaxial necking in a tension test. Adding to the complexity of pull-out plasticity, the applied force must overcome the frictional resistance at the fibre bend when interfaced with coarse aggregate and also account for any relief in that force from the freed interface surface arising from the spalling that occurs. In combination it would appear that the respective changes to the force amount to a cancellation of such spurious influences upon it, consistent with the force bounding estimates given here.

4. Bounding Model Refinements

In order to ascertain the reliability of the proposed approach to describe the failure of inclined hooked end fibres, various experimental results from data published in the literature [26–28] have been compared with the bounds found from Equations (3) and (6b). The experimental data have been chosen primarily to enable an account of the embedded strength of hooked-end fibre with different shank orientation. Other variables include fibre diameter, the tensile strength of the fibre and the compressive strength of the concrete. In the experiments the embedded shank half-length has varied together with its hook end geometry. The upper bound (u. b.) does not require these specific details explicitly only that the hook should provide sufficient anchorage for a shank failure to occur. Diameter appears in the calculation for the nominal stress σ_θ under the applied force and diameter is also maintained in testing fibre for the tensile and shear strength assessments described above. Concrete strength is important to an u. b. estimate, the latter being lowered by bending when spalling occurs in a weaker matrix composition. Embedded length influences any slip that occurs but does not contribute to the shank failure load or the σ_θ calculation. The normalised unit ordinate in each of Figs 6a-d indicates that if a shank failure should occur in aligned failure it would do so at a force corresponding to the fibre's UTS. Hence the normalised ordinate intercept of unity shown marks the start of all u. b. plots. This intercept refers to a pure (unlikely) tensile failure of aligned fibre and is therefore independent of the matrix composition. With increasing fibre mis-alignment to the force the u. b. plot of transversely isotropic fibre depends upon orientation in a manner controlled by its two strength ratios. Figure 10 examines the upper bound estimates in more detail. Five combinations of pairs of strength ratios are sufficient to show that the experimental data are captured by these u. b. plots. It is noted that u. b. plots may rise or fall from its unit intercept in the manner shown depending upon the strength combination chosen in Figure 10. This figure presents from Equation (3) upper bounds to the strength dependency of transversely isotropic fibre with embedded orientation. In Figure 10 anisotropic, off -axis plots apply to strength ratios typical of cold drawn high strength metallic fibre. Specific strength ratios that appear are taken from the ranges:

Preprints.org (www.preprints.org) | NOT PEER-REVIEWED | Posted: 11 June 2024 doi:10.20944/preprints202406.0617.v1

$$1 \leq \frac{\sigma_{1f}}{\sigma_{2f}} \leq 3 \text{ and } \frac{1}{2} \leq \frac{\sigma_{2f}}{\sigma_{12f}} \leq 1\frac{1}{2}$$

Overlaid upon the five u. b. plots in Figure 10 are the available experimental data. The five upper bound predictions shown apply to their two strength ratios lying in the ranges:

$$1 \leq \frac{\sigma_{1f}}{\sigma_{2f}} \leq 1\frac{1}{2} \text{ and } \frac{1}{2} \leq \frac{\sigma_{1f}}{\sigma_{12f}} \leq \frac{3}{4}.$$

Overall, the experimental data agrees mostly with a strength ratio combination of $\frac{\sigma_{1f}}{\sigma_{2f}} = 1\frac{1}{2}$ and $\frac{\sigma_{1f}}{\sigma_{12f}} = \frac{3}{4}$. For the new data (o) the reduction to upper bound strength at and beyond the 30° inclination angle has been attributed to matrix spalling during the pull-out process. With the change from lower to upper bound the fibre fails from having attained its off-axis combined strength under the applied force.

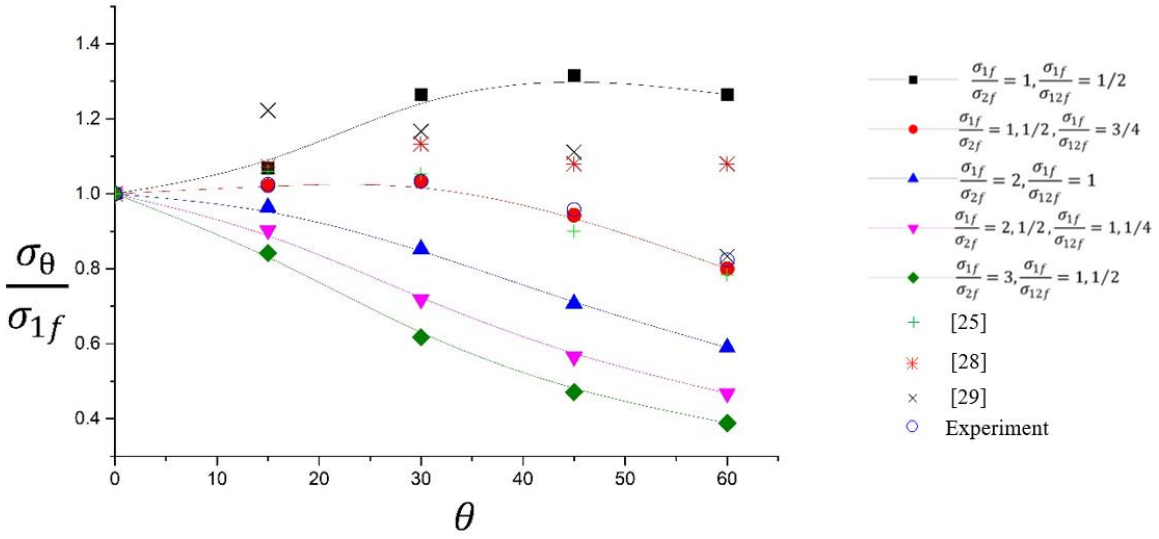

Figure 10. Strength dependency of transversely isotropic fibre upon embedded orientation. Comparisons between Equation 3, experiment (o) and other published data.

Considerably more experimental data [31] are available for aligned fibre where lower bound force/stress estimates apply to a complete pull-out. Further data [31–33] suggests that fibres will pull out when embedded with a slight mis-alignment to the force. In Fig 6, for example, the lower bound peak force attained has been converted to a nominal stress and then normalised with the fibre's axial tensile strength (see Equations 6a, b). Results (which include aligned fibre, $\theta = 0^{\circ}$), show that the ultimate tensile strength of the fibre material is *never reached* under the peak load required to straighten the hook for complete pull out to occur. Therefore, the aligned fibre results indicate an intercept value of less than unity to be placed upon the ordinate in Figure 10. This marks that start of the lower bound plot that rises in proportion to $1/\cos\theta$ for a narrow orientation range. Here, Figs 6a-d have shown the range that applies to l. b plots for four composites in which each aligned fibre-cement combination has a different intercept on the stress axis. Hence the intercepts for each u .b. plot depend upon the fibre-cement combination[34].. In contrast each u. b plot in Figure 10 has a common intercept of unity at the UTS of the fibre.

5. Conclusions

In this paper a new bounding approach has been developed to predict the pull-out response of misaligned hooked-end steel fibre embedded in a concrete matrix. An upper bound estimate to the pull-out strength is based upon a transversely isotropic failure condition arising in the straight length of the inclined fibre shank. That bound accounts for orientation and strength properties of the deep drawn fibre. The transversely isotropic failure criterion applies to deep drawn wire having grains

 doi:10.20944/preprints202406.0617.v1

elongated by multiple reductions to its final diameter. Metallography revealed that elongated grains, with an aspect ratio exceeding five, were aligned with the fibre's length direction. An upper bound to the interrupted pull-out failure of an embedded, inclined fibre accounts for its anisotropic strength under the off-axis plane stress state that exists within its shank. Fibre strength tests have been proposed to measure the transverse strength and the shear strengths required for setting an upper bound limit curve. A lower bound limit is based upon the complete pull-out of an aligned, hooked end fibre embedded in a cementitious matrix. There the peak force is associated with that force required to straighten the hook end. Therein experimental data are used to set the peak nominal stress (force/area) limit initially for an aligned fibre. For inclined fibre that stress increases with it being inversely proportional to the cosine of an inclination angle. Normally, in a strong matrix the lower bound mode is restricted to a range 0 – 30. Beyond this range fibre failure occurs in the upper bound mode in which the shank yields. However, a lower bound mode range may be extended where matrix spalling allows the fibre to bend in closer alignment with the pulling force. This applies provided such bending does not result in fibre breakage where then it has contributed to an upper bound failure. It is suggested here that a further intermediate bound be placed upon the strength of the concrete mix in the interface region where spalling occurs. Consideration of the u.b. and l.b. modes of failure proposed here and the division arising between them has provided, this far, an explanation of all available experimental data. Finally, the motivation for the present study has been to admit a two-mode failure analysis of misaligned hooked-end steel fibre. Such behavior is relevant to concrete reinforcement with short fibre having random orientation as for pre-cast concrete sections say for tunnels and a viaduct. Where loading is complex and the random fibre orientation ensures some alignment with varying principal stress directions. In contrast, the r-bar reinforcement of beams and columns is aligned with the unvarying direction of maximum tension.

References

1. Wang, Y.; Hao, Y.; Hao, H.; Huang, X. An efficient method to derive statistical mechanical properties of concrete reinforced with spiral-shaped steel fibres in dynamic tension. *Constr Build Mater* **2016**, *124*, 732-745.
2. Zīle, E.; Zīle, O. Effect of the fiber geometry on the pullout response of mechanically deformed steel fibers. *Cem Concr Res* **2013**, *44*, 18-24.
3. Tai, Y.; El-Tawil, S. High loading-rate pullout behavior of inclined deformed steel fibers embedded in ultra-high performance concrete. *Constr Build Mater* **2017**, *148*, 204-218.
4. Khalifa, A.; El-Thakeb, A.E.-W.; El-Sebai, A.; Elmannaey, A. Innovative Flexural Repair Technique of Pre-Damaged T-Beams Using Eco-Friendly Steel-Fibre-Reinforced Geopolymer Concrete. Fibers 2024, 12, 3. https://doi.org/10.3390/fib12010003.
5. Mujalli, M.A.; Dirar, S.; Mushtaha, E.; Hussien, A.; Maksoud, A. Evaluation of the Tensile Characteristics and Bond Behaviour of Steel Fibre-Reinforced Concrete: An Overview. Fibers 2022, 10, 104. https://doi.org/10.3390/fib10120104.
6. Feng, J.; Sun, W.W.; Wang, X.M.; Shi, X.Y. Mechanical analyses of hooked fiber pullout performance in ultra-high-performance concrete. *Constr Build Mater* **2014**, *69*, 403-410.
7. Abu-Lebdeh, T.; Hamoush, S.; Heard, W.; Zornig, B. Effect of matrix strength on pullout behavior of steel fiber reinforced very-high strength concrete composites. *Constr Build Mater* **2011**, *25*, 39-46.
8. Tuyan, M.; Yazici, H. Pull out brhaviour of single steel fibre from SIFCON matrix. Constr Build Mater. 2012, 35, 571-577.
9. Beglarigale, A.; Yazıcı, H. Pull-out behavior of steel fiber embedded in flowable RPC and ordinary mortar. *Constr Build Mater* **2015**, *75*, 255-265.
10. Won, J.; Hong, B.; Lee, S.; Choi, S.J. Bonding properties of amorphous micro-steel fibre-reinforced cementitious composites. *Composite Structures* **2013**, *102*, 101-109.
11. Won, J.; Lee, J.; Lee, S. Bonding behaviour of arch-type steel fibres in a cementitious composite. *Composite Structures* **2015**, *133*, 117-123.
12. Luck, J.D.; Bazli, M.; Rajabipour, A. Bond between Fibre-Reinforced Polymer Tubes and Sea Water Sea Sand Concrete: Mechanisms and Effective Parameters: Critical Overview and Discussion. Fibers 2022, 10, 8. https://doi.org/10.3390/fib10010008.
13. Al-Abdaly, N.M.; Hussein, M.J.; Imran, H.; Henedy, S.N.; Bernardo, L.F.A.; Al-Khafaji, Z. Shear Strength Prediction of Steel-Fiber-Reinforced Concrete Beams Using the M5P Model. Fibers 2023, 11, 37. https://doi.org/10.3390/fib11050037.

 doi:10.20944/preprints202406.0617.v1

14. Abrishambaf, A.; Barros, J.A.O.; Cunha, Vitor, M. C. F.; Frazão, C. Time dependent behaviour of fibre pull-out in self-compacting concrete. *Cement and Concrete Composites* **2017**, *77*, 14-28, DOI 10.1016/j.cemconcomp.2016.12.004. Available online: http://www.sciencedirect.com/science/article/pii/S0958946516308174.
15. Georgiadi-Stefanidi, K.; Mistakidis, E.; Pantousa, D.; Zygomalas, M. Numerical modelling of the pull-out of hooked steel fibres from high-strength cementitious matrix, supplemented by experimental results. *Constr Build Mater* **2010**, *24*, 2489-2506.
16. Chanvillard, G. Modeling the pullout of wire-drawn steel fibers. *Cem Concr Res* **1999**, *29*, 1027-1037.
17. Alwan, J.M.; Naaman, A.E.; Guerrero, P. Effect of mechanical clamping on the pull-out response of hooked steel fibers embedded in cementitious matrices. *Concrete Science and Engineering* **1999**, *1*, 15-25.
18. Laranjeira, F.; Aguado, A.; Molins, C. Predicting the pullout response of inclined straight steel fibers. *Mater Struct* **2010**, *43*, 875-895.
19. Soetens, T.; Van Gysel, A.; Matthys, S.; Taerwe, L. A semi-analytical model to predict the pull-out behaviour of inclined hooked-end steel fibres. *Constr Build Mater* **2013**, *43*, 253-265.
20. Lee, Y.; Kang, S.; Kim, J. Pullout behavior of inclined steel fiber in an ultra-high strength cementitious matrix. *Constr Build Mater* **2010**, *24*, 2030-2041.
21. Laranjeira, F.; Molins, C.; Aguado, A. Predicting the pullout response of inclined hooked steel fibers. *Cem Concr Res* **2010**, *40*, 1471-1487.
22. Zhan, Y.; Meschke, G. Analytical model for the pullout behavior of straight and hooked-end steel fibers. *J Eng Mech* **2014**, *140*, 04014091.
23. Rees, D.W. *Mechanics of Solids and Structures*, World Scientific Publishing Co Inc: 2016.
24. Jones, R.M. Mechanics of Composite Materials, CRC press: 1998.
25. Isla, F.; Ruano, G.; Luccioni, B. Analysis of steel fibers pull-out. Experimental study. Constr Build Mater 2015, 100, 183-193.
26. Rees, D.W. Mechanics of Elastic Solids, World Scientific: 2018.
27. Rees, D.W. *Handbook on Mechanics of Inelastic Solids*, Vol. 2, Chapter13, World Scientific, 2023.
28. Robins, P.; Austin, S.; Jones, P. Pull-out behaviour of hooked steel fibres. *Mater Struct* **2002**, *35*, 434-442.
29. Van Gysel, A. Studie van het uittrekgedrag van staalvezels ingebed in een cementgebonden matrix met toepassing op staalvezelbeton onderworpen aan buiging. *status: published* **2000**.
30. Yu, Tongxi, and Pu Xue. Introduction to Engineering Plasticity: Fundamentals with Applications in Metal Forming, Limit Analysis and Energy Absorption. Elsevier, 2022.
31. Abdullah, S.M. Bonding Mechanisms and Strength of Hooked-End Steel Fibre Reinforced Cementitious Matrix, Ph. D. thesis, Brunel University, 2017.
32. Abdullah, S, Fan, M, and Rees, D.W.A. Predicting pull-out behaviour of 4D/5D hooked end fibres embedded in normal high strength concrete.
33. Ding, X.; Zhao, M.; Li, H.; Zhang, Y.; Liu, Y.; Zhao, S. Bond Behaviors of Steel Fiber in Mortar Affected by Inclination Angle and Fiber Spacing. Materials 2022, 15, 6024. https://doi.org/10.3390/ma15176024.
34. MacGregor, J.G. and Wight, J.K. Reinforced Concrete, Mechanics and Design. fourth Edition, 2005, Prentice-Hall.